Integral Effects of Deep Convection

UWE SEND

Institut für Meereskunde, Kiel, Germany

JOHN MARSHALL

Center for Meteorology and Physical Oceanography, Department of Earth, Atmospheric and Planetary Sciences, Massachusetts Institute of Technology, Cambridge, Massachusetts

(Manuscript received 1 April 1993, in final form 1 August 1994)

ABSTRACT

The large-scale, integral effect of convective elements (plumes) constituting an open-ocean chimney is investigated both theoretically and with a plume-resolving numerical model. The authors consider an initially homogeneous "patch" of ocean of depth H, with Coriolis parameter f, in which buoyancy is lost from the surface at a rate B. Both vorticity constraints on the convection patch and model analyses imply that, irrespective of the details of the plumes themselves, the mean vertical transport resulting from their action must be vanishingly small. Plumes are best thought of as mixing agents, which efficiently homogenize properties of the chimney.

Scaling laws are derived from dynamical arguments and tested against the model. Using an expression for the vertical mixing timescale, they relate the chimney properties, the strength of the geostrophic rim-current setup around it, and its breakup timescale by baroclinic instability to the external parameters B, f, and H. After breakup, the instability eddies may merge to form larger "cones" of convected water, which offset the buoyancy loss at the surface by laterally incorporating stratified fluid. Properties of the plumes only enter the scaling results by setting the vertical mixing timescale.

The authors argue that the plume scale may be parameterized by a mixing scheme if this implies the appropriate mixing timescale. Finally, the authors suggest that for the estimation of deep-water formation rates the volume of convectively modified fluid processed by a chimney should be computed rather than the mean vertical transport during the convection phase.

1. Introduction

Deep-water formation by convective processes has been observed in several parts of the World Ocean using a number of different means. The prime focus of such studies has been the Mediterranean "MEDOC" region because of its accessibility and predictability (convection seems to occur in the same place roughly the same time every year). The first clear documented evidence of deep-reaching convection in the Mediterranean was obtained by the MEDOC Group (1970), who observed a large patch of extremely homogeneous water after a strong cooling event. This type of observation was repeated in later years by further experiments of the MEDOC Group (1970), Gascard (1973), by Leaman and Schott (1991), and most recently by a European consortium in the winter of 1991/92 (The THETIS Group 1994). Direct evidence of large convective downward water motion has been provided by float measurements of Voorhis and Webb (1970) and by moored Acoustic Doppler Current Profiler (ADCP) time series of Schott and Leaman (1991). The reported vertical velocities reached values of 10 cm s^{-1}, and Schott and Leaman obtained average downward speeds $\bar{w}$ of 1 cm s^{-1} during the convection period. [Observations in the Greenland Sea, by contrast, showed no significant $\bar{w}$ (Schott et al. 1993).] Those moored time series also revealed that the space scale of the convective motions seemed to be of the order of 1 km, which is believed to represent the individual plumes carrying the dense water, which had been cooled at the surface, downward.

Laboratory experiments (Maxworthy and Narimousa 1994; Brickman and Kelley 1993) and numerical modeling efforts (Jones and Marshall 1993, henceforth JM) together with the aforementioned field observations, suggest complex hydrodynamical mechanisms at work involving a variety of scales and processes: the convection patch (or "chimney") set by the preconditioning and cooling (scale typically a 50–100 km), the instabilities of the patch developing eddies and cones[1] on the periphery of the patch (5–10 km

Corresponding author address: Dr. Uwe Send, Institut für Meereskunde, an der Universität Kiel, Düsternbrooker Weg 20, Kiel D-24105, Germany.

[1] The term "cones" has been used to describe the eddies of dense water that have detached from the chimney after breakup. Due to the inclined isopycnals from rotational adjustment, they have a cone-shaped cross section (see Fig. 10). They develop originally from the instability eddies but are distinct from them.

scale), and the convection plumes themselves (1 km scale). These papers also put forward a variety of scaling ideas for the properties of the plumes and cones based on external parameters.

In the present study, we are concerned with the integral effect of a population of plumes. We suggest that the convection itself is best thought of as a mixing agent that overturns the convective column and efficiently homogenizes it. While the plumes themselves represent very interesting phenomena and dynamics, here we seek to address the net large-scale effect of a population of plumes on the convection patch in order to learn how to estimate and efficiently model the large-scale consequences of convection for the circulation and deep-water mass formation rates. Indeed, our main conclusions are largely independent of the details and dynamics of the plumes themselves. The implications of our study for strategies to parameterize convection in models and to observe the process in the field are also discussed.

To focus our ideas and test our large-scale scalings, we make much use of numerical experiments using the nonhydrostatic model of JM, which explicitly resolve rather than parameterize the convective overturning of a chimney. Appropriate integral properties of those experiments are diagnosed in detail and, where necessary, further experiments are carried out. The study only addresses the convective phase and the subsequent breakup of the chimney (or patch) of dense fluid into eddies (cones). The dispersal and ultimate assimilation of this dense convected water into the general circulation is not considered here.

2. Plumes: vertical conduits or mixing elements?

We inquire here into the integral effect of a population of convective plumes. In terms of their dynamic role, one can envisage two different scenarios. In the first, the plumes act as *conduits* that transport cooled heavy water downward and thus represent the main mechanism for transport of water vertically and deep-water renewal. The other possibility is that the population of plumes merely acts as an efficient *mixing agent*, stirring the water column top to bottom, but without having a significant net vertical transport. Each view would have important consequences dynamically and for the way one would estimate deep-water formation rates from observations and parameterize such convection regimes in models. We will address each possibility in turn.

a. Conduits

Figure 1a(top) sketches the scenario suggested by the conduit view of plumes. There are large downward velocities within the plumes. In between there is upwelling that, however, does not locally compensate the downward transport of the plumes. As a result, there is a net mean vertical velocity $\bar{w}$ in the interior of the convection patch, and this water has to be supplied by a convergence at the surface with an outflow of (new deep) water at the bottom.

We can estimate typical magnitudes suggested by this picture to see if it seems reasonable. Schott and Leaman (1991) measure vertical velocities of 10 cm s^{-1} downward inside the plumes, which is the same order of magnitude as the plume velocities seen in the modeling study of JM and in accord with scaling estimates presented there. In between, upward motions are observed. Over a period of intense cooling lasting one week, Schott and Leaman observed at their mooring a mean downwelling of 1 cm s^{-1}. If one assumes that this is representative of $\bar{w}$ over the whole chimney, some 50 km in diameter, this produces 20 Sv (Sv $\equiv 10^6$ m^3 s^{-1}) of deep water during that week or 0.4 Sv if one such event is averaged over one year. This is a plausible number given the currently accepted deep-water formation rate (Bryden and Stommel 1982) and suggests that all the deep water can be produced in a short ($\sim$1 week) period of intense downwelling.

There are, however, vorticity constraints on the downward motion, which suggest that the above picture is unphysical. The surface convergence [Fig. 1a(top)] would stretch fluid columns in the upper layer and squash tubes in the lower layer, spinning up cyclonic relative vorticity above and anticyclonic currents below, according to the linear vorticity balance

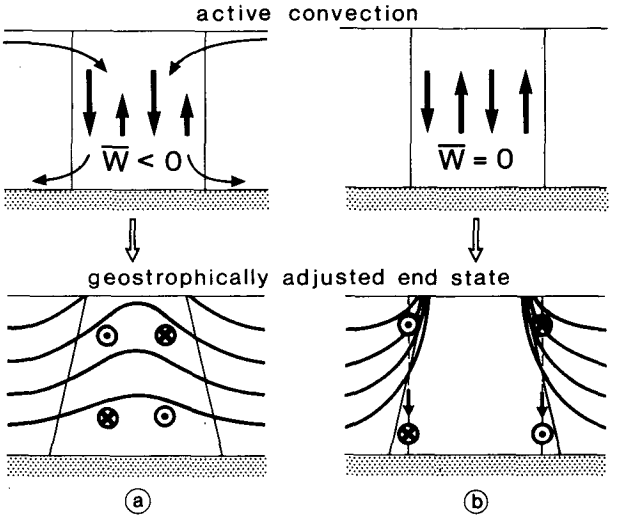

FIG. 1. The two idealized scenarios for a convection patch. The active convection phase with vertical (plume) motion is sketched in the upper panels; the subsequent geostrophically adjusted state is indicated with density contours below. (a) Case with net downward motion from the plumes, associated inflow (convergence) at surface, and outflow (divergence) at bottom. (b) Compensation of downward plume velocities with zero vertical transport. During subsequent adjustment, the slumping of the sidewalls, however, represents a mean w.

$$\frac{\partial \bar{\zeta}}{\partial t} = f \frac{\partial \bar{w}}{\partial z}, \tag{1}$$

where ζ is the relative vorticity, f is the Coriolis parameter, w is the vertical velocity, and $(\cdots)$ denotes an average over the patch.

Using the above numbers, $\partial \bar{w}/\partial z = 1$ cm s^{-1}/1000 m sustained for a period of 1 week, we obtain an average relative vorticity of $\bar{\zeta} = 6f$. This would correspond to interior shears of the order of 3 m s^{-1} over 10-km regions. We can also estimate the circulation around the convection patch, or the so-called "rim current," from the integrated vorticity inside:

$$u_{\text{rim}} = \frac{R\bar{\zeta}}{2} \sim \frac{Rf\bar{w}}{H} t, \tag{2a}$$

where R is the radius of the convection patch. Inserting the same numerical values, we obtain $u_{\text{rim}} = 7.5$ m s^{-1} if $R = 25$ km. Such large-scale vorticity and velocity scales are very unrealistic. One must conclude that the vertical motion inside the plumes is almost entirely compensated by upwelling in between (i.e., $\bar{w} \sim 0$), as sketched in Fig. 1b (top), representing the "mixing element" view of convection.

A signature of the role of the plumes can also be seen in the density field. Again, suppose for a moment that there were a significant $\bar{w}$ in the interior; then the cyclonic/anticyclonic vorticity shear generated by it everywhere in the interior would adjust to thermal wind balance within an inertial period, resulting in a density field as schematized in Fig. 1a (bottom). Thus, horizontal density gradients inside the convection patch would be an indicator of the presence of mean vorticity and hence vortex stretching through systematic downwelling. Data collected inside the patch during many convection events since the MEDOC experiments show, however, that the patch is very homogeneous on the large scale, more in accord with the mixing scenario sketched in Fig. 1b (bottom). This, again, supports the observation that the mean vertical velocity in the interior of the patch is vanishingly small. Thus, apparently the plumes mainly act to mix the water column vertically and do not act as the primary mechanism of net vertical mass transfer.

b. *Mixing elements*

Let us now consider the consequences if the plumes only act to mix the water vertically. The simplest possible scenario would be a two-stage process in which, first, the convection cools and mixes a patch of water during a time short compared to the inertial timescale, creating a dense homogeneous cylinder of fluid that, second then collapses and adjusts under gravity and rotation (see Fig. 1b). Dewar and Killworth (1990) and Herman and Owens (1993) have studied this idealized problem, and the net result is, not surprisingly, a lateral displacement of the interface (inward

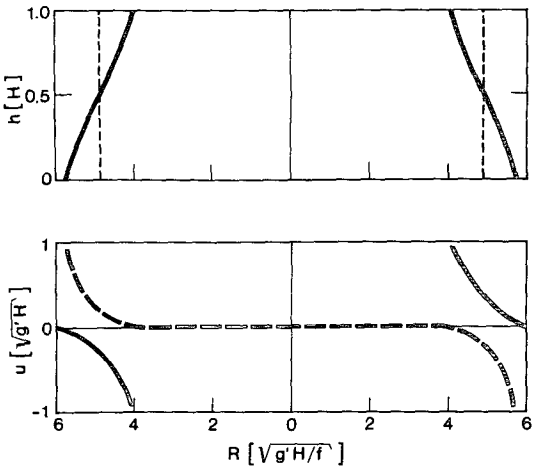

FIG. 2. Example solution of the equations given in Dewar and Killworth (1990) for the strip collapse, which asymptotes to the cylinder collapse for cylinders of several Rossby radii in size. Top: Interface shape before and after collapse. Bottom: current in upper/outer layer (solid) and in lower/interior layer (dashed). If cooling is applied continuously within the original cylinder region, the adjustment will continually bring new water into the region at the surface. The new water is exposed to cooling, thus setting up a smooth gradient rather than a discontinuous jump in density in the upper layer. Similarly, a gradient instead of the sharp interface shown here will arise in the lower layer due to the continued outward movement and simultaneous cooling.

at the top, outward at the bottom) by a horizontal distance of the order of a Rossby deformation radius $L_\rho = \sqrt{g'H}/f$ (see Fig. 2 for an analytical solution). Here $g' = Bt/H$ is the reduced gravity resulting from cooling at the surface with the buoyancy flux B for a time t and mixing the column over the depth H. The slumping of the interface, implying a vertical transport, generates vorticity in the vicinity of the interface, that is, in a circular strip of width L_ρ. The velocities are of order $\sqrt{g'H}$ in this discrete two-fluid solution with density and velocity discontinuities across the interface. We can obtain a "smoother" scaling by allowing, instead, a continuous density variation across the zone of width L_ρ. Then, applying thermal wind balance to a vertical shear of u_{rim} over a depth of $H/2$ yields[2]

$$u_{\text{rim}} = \frac{1}{2}\sqrt{g'H} = \frac{1}{2}\sqrt{Bt}. \tag{2b}$$

Let us again insert typical observed values. The buoyancy flux typical of open-ocean convection sites—see Table 1 below—has an order of magnitude of 10^{-7} m^2 s^{-3}, corresponding to a heat flux of $\sim$250 W m^{-2}. Applying this cooling rate for one week would result

[2] In Dewar and Killworth (1990), $H/2$ is the (mean) thickness of the two layers and u_{rim} is the shear between the layers—the maximum current in the top and bottom layers are offset sideways (see Fig. 2). In our model runs, u_{rim} decays to zero or reverses at middepth, i.e., again the shear is u_{rim} over $H/2$.

TABLE 1. Small-scale plume properties suggested by the scaling reviewed in JM in the open-ocean deep convection regime for $H = 2$ km, $f = 10^{-4}$ s^{-1}. The typical scale of the convective plumes is l_{rot}, the magnitude of the attendant currents is u_{rot}, and l_p is the radius of deformation set up by the convective elements.

		Q (W m^{-2})			
		100	500	1000	1500
		B (m^2 s^{-3})			
Scaling		5.00×10^{-8}	2.5×10^{-7}	5.00×10^{-7}	7.5×10^{-7}
l_{rot}(km)	$\left(\frac{B}{f^3}\right)^{1/2}$	0.22	0.47	0.71	0.85
u_{rot}(m s^{-1})	$\left(\frac{B}{f}\right)^{1/2}$	0.02	0.05	0.07	0.09
l_p(km)	$\frac{B^{1/4}H^{1/2}}{f^{3/4}}$	0.67	0.97	1.19	1.31
R_o^*	$\frac{B^{1/2}}{f^{3/2}H}$	0.11	0.24	0.35	0.43

in $u_{rim} = 12.5$ cm s^{-1} by (2b), which is a reasonable current and in accord with observations. Of course, such an extended period of cooling violates our initial assumption, so we ought to consider a very strong event for a short period—we obtain the same answer because it is the product Bt, the total buoyancy extracted, that matters. There is an average vertical velocity inside the cooling region, but it is localized at the edge of the patch and is a consequence of the slumping during the adjustment process. Its magnitude can be estimated from the volume of water that has moved inwards at the surface by the distance of a deformation radius L_ρ. Approximating the cross section of this volume as a triangle of base L_ρ and height $H/2$, the volume is $2\pi RL_\rho H/4$. For continuity this water must move downward across the depth level $H/2$, and averaged over the patch we thus obtain

$$\bar{w} = \frac{H}{2fR}\sqrt{B/t} = \frac{H}{fR}\frac{u_{rim}}{t}, \qquad (3)$$

where u_{rim} from above has been substituted from Eq. (2b). This result (derived only from the cylinder collapse solution together with volume conservation) is in agreement with (2a), which was obtained using the linear vorticity balance (1). Thus, in the context of the cylinder collapse problem, the geostrophic rim current can be understood by (and fulfills) a simple linear vorticity balance. Equation (3) implies a $\bar{w} = 1$ mm s^{-1} if the buoyancy is extracted very intensely during 1 day or 0.15 mm s^{-1} if the same amount of buoyancy is extracted over 1 week ($H = 2$ km and $R = 25$ km as above). This would be a volume flux of 0.3 Sv on average during the week or only 0.005 Sv over a year.

Thus, adopting a mixing-element view of a plume population, we arrive at vorticity and velocity scales that are more realistic. Furthermore, it is clear that the $\bar{w}$ implied by this process cannot account for the observed deep-water formation rates. A more appropriate way of estimating the rate at which water is formed by the chimney is to compute the volume of fluid processed by it—this will be considered in section 5.

c. *Inferences from explicit numerical simulations of convection*

The numerical simulations of JM, which addressed convection in the presence of rotation in a neutral ocean and in a weakly stratified ocean, strongly support the "mixing agent" view of convection and will be analyzed and extended here. Jones and Marshall presented scaling arguments for the plume and cone dynamics, which found broad support from numerical experiments. A measure of the importance of rotation on the convective process was provided by a natural Rossby number used by Maxworthy and Narimousa (1994), JM, and Marshall et al. (1994):

$$R_o^* = \frac{l_{rot}}{H} = \frac{u_{rot}}{fH} = \frac{B^{1/2}}{f^{3/2}H},$$

where $l_{rot} = (B/f^3)^{1/2}$ is the length scale, which marks the transition from three-dimensional, thermally driven turbulence to quasi-two-dimensional, rotationally dominated motions. Here, $u_{rot} = (B/f)^{1/2}$ is the velocity of a particle gyrating in inertial circles of radius l_{rot} and was shown to set the horizontal and vertical velocity scale for the plumes.

In the parameter regime typical of open-ocean deep convection, $R_o^* \leq 1$ (see Table 1 of JM reproduced above, which gives typical space and velocity scales), and rotation influences the intensity and scale of both the convective plumes and the instability eddies that form in the rim current around the

periphery of the convection patch. These eddies then form the cones of geostrophically adjusted convected water that break off from the convection region. In particular, the scale, intensity, and buoyancy excess of the plumes and eddies were found to depend in a predictable way on this single nondimensional number, formed from the external parameters f, B, and H.

Our focus here, however, is on the integral effects of a patch of convection and, in particular, whether the plumes are best thought of as mixing agents or "conduits." In Fig. 3 we present a hydrographic section through the center of a simulation of a chimney of radius 8 km, illustrating the vertical velocity field of the plumes in a weakly stratified ocean, cooled at the surface at a rate $B = 3.6 \times 10^{-7}$ m^2 s^{-3} (corresponding to a heat loss of 800 W m^2). This simulation is discussed in JM in some detail (see section 6 of JM). Plumes of dense fluid can be seen "raining down" from a dense surface boundary layer. Downwelling velocities exceed 10 cm s^{-1} but, as we shall see, are compensated by upwelling velocities in between.

In Fig. 4 we plot w (at 500 m) and ζ (at 50 m) at two days after cooling commenced. In the interior of the patch there is vorticity generated on the individual plume scale as a consequence of the organized downward and upward flow inside the plumes, according to (1). The w and vorticity field, although granular in nature, is a mix of cells of opposite sign. We see intense regions of cyclonic circulation associated with downwelling, but adjacent to and in between there is anticyclonic circulation in (somewhat more extended) regions of compensating upwelling.

In Fig. 5 we analyze the integrated relative vorticity and vertical velocity induced by the convection; the upper-layer relative vorticity and vertical velocity are presented as a *cumulative* integral over discs as a function of the radius of the discs from the center of the convection patch (which had a radius of 8 km as in all simulations shown here). The integral is necessary to smooth out the noisy interior field and at the same time is a convenient measure directly yielding the circulation around the region (Fig. 5a) and the vertical transport (Fig. 5b). The most conspicuous feature of Fig. 5 is the concentration of vorticity and vertical velocity at the edge of the cooling region, with positive vorticity (downward w) in the inner side and negative vorticity (upward w) on the outer side of the rim current. The rim current calculated from the maximum area-integrated vorticity in this figure is approximately 11 cm s^{-1}. Outside this thin region, average vertical motion and vorticity, both in the interior and outside the patch, are vanishingly small. Thus, in the interior, w [and by (1) also ζ] averages to zero due to the small-scale compensating motions evident in Fig. 4 and 5. The vertical velocity amplitudes seen in Fig. 5b are consistent with the vorticity generation seen in Fig. 5a, according to (1).

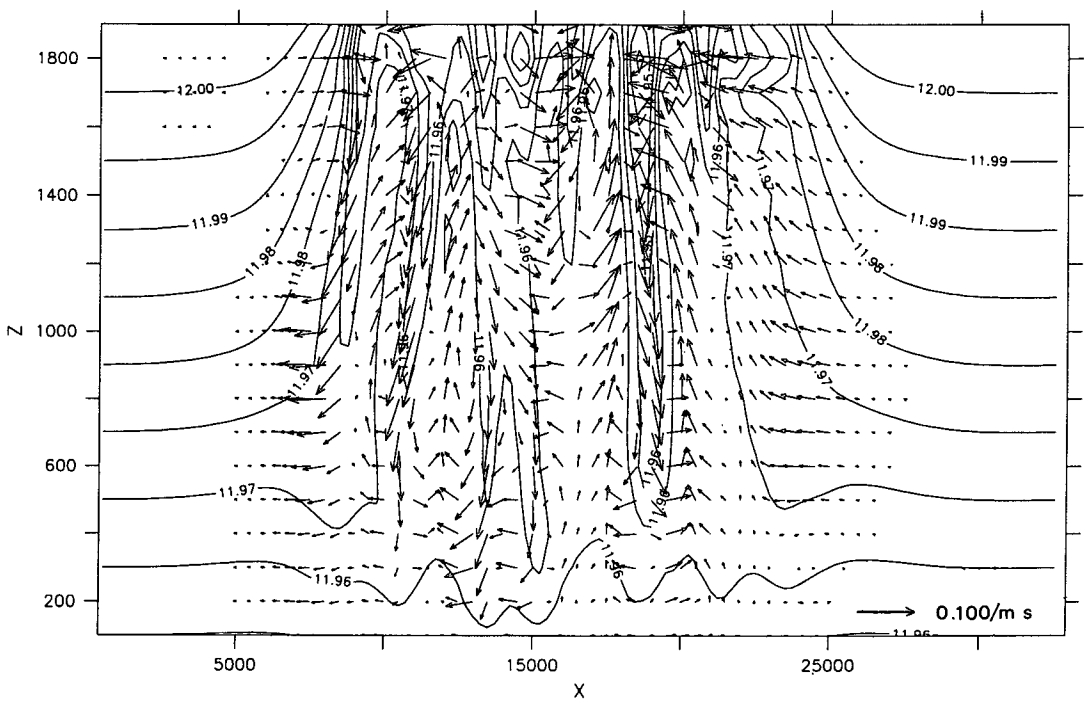

FIG. 3. Cross section through the weakly stratified reference run of JM illustrating plume development and shape. Plotted are temperature contours and current vectors.

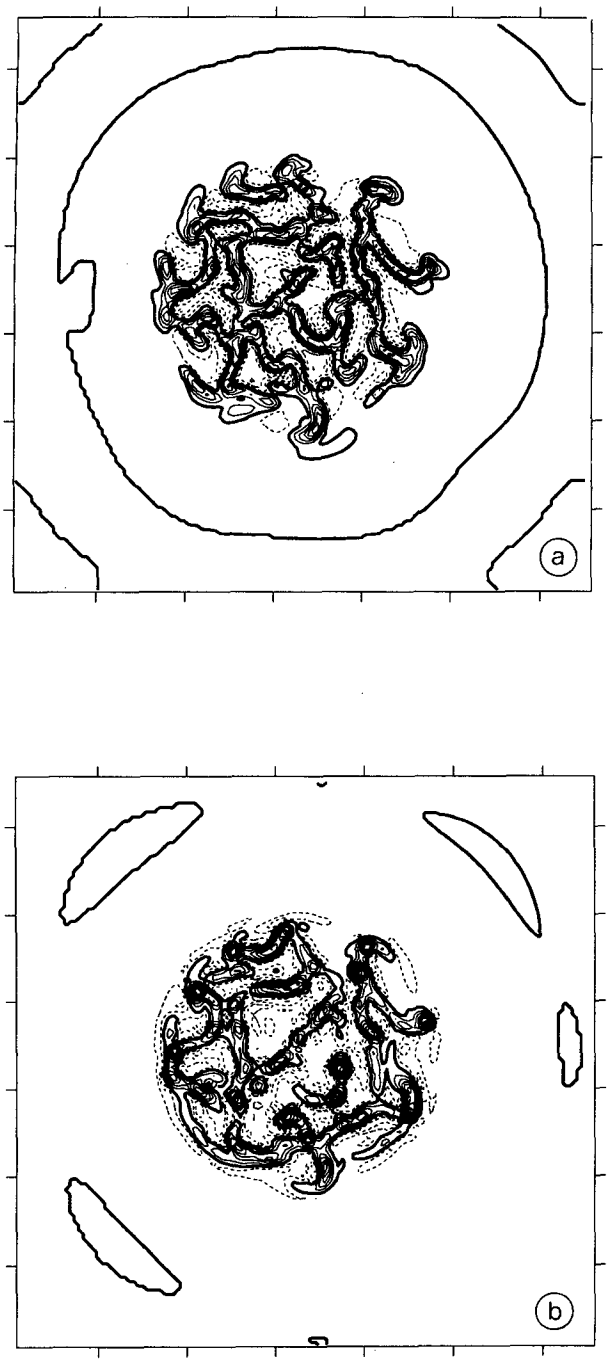

FIG. 4. Horizontal sections through the simulation shown in Fig. 3, showing the whole x–y model domain of 32-km size. (a) Vertical velocity at a depth of 500 m, contour interval is 2 cm s^{-1}. Intense, small-scale downward motion (solid contours) of the plumes is clearly seen, with weaker but more widespread upward motions (dashed contours) in between. Close to the edge of the patch, an absence of upward motion is just visible, which gives rise to the net downward transport there. (b) Relative vorticity at 50 m, contour interval 6 $\times 10^{-5}$ s^{-1}. Strong positive values (solid) are found associated with the plumes seen in (a) and weaker negative values (dashed) between. Again, an absence of compensating negative values is seen near the edge. However, the average residual values are masked by the large, small-scale variability.

Although Fig. 5 shows a weakly stratified calculation, the cylinder collapse solution and the scaling laws presented in JM were derived for the problem of convection in an unstratified fluid. We have also diagnosed the same quantities as in Fig. 5 from the "reference" experiment of JM, which simulated the convective overturning of an unstratified ocean (all the other parameters of the simulation remained the same). The generated rim current and its time evolution until the end of the cooling at 2 days is within 10% of the weakly stratified case shown in Fig. 5. Thus, the observed rim current agrees with the expectation from cylinder collapse ($u_{\text{rim}} = \frac{1}{2}\sqrt{Bt} = 12.5$ cm s^{-1}) and will also be shown to be in accord with scaling laws derived in section 3b. We present the stratified case here to demonstrate the applicability of our basic statements to weakly stratified ($N \sim f$) as well as neutral conditions.

In summary, then, explicit calculations show, both qualitatively and quantitatively, that the principle function of the plumes is to mix the column in accord with the schema presented in Fig. 1b rather than 1a. Thus, theoretical considerations, observations, and numerical simulations all support the "mixing element" view of plumes. Before discussing some of the implications—for estimation of deep-water formation rates and for parameterization of convection in large-scale models (see section 5)—we now go on to consider further integral properties of the chimney. Of particular interest is the mixing timescale and the magnitude of the rim current induced around the periphery of the convecting chimney.

3. Integral properties of the chimney

a. Vertical mixing timescale

The plumes shown in Fig. 3 take a finite time to carry water to the bottom at a speed close to u_{rot} defined in Table 1. Thus, vertical mixing does not take place instantaneously; homogenization occurs on a timescale set by the vertical plume velocities and the depth of the ocean. Since we have argued above that adjustment under rotation and gravity is the main mechanism for vertical velocity and vorticity generation, the relation of the adjustment timescale ($2\pi/f$) to the mixing timescale must play a role in determining the properties of the regime. A measure of the mixing (or overturning) timescale is the time, which we shall call t_{mix}, it takes for a plume to reach the bottom at depth H (in a stratified fluid H would be interpreted as the local depth of the convective mixed layer),

$$t_{\text{mix}} \sim \frac{H}{w_{\text{plume}}} \sim HB^{-1/2}f^{1/2}, \qquad (4)$$

assuming that $w_{\text{plume}} \sim u_{\text{rot}} = (B/f)^{1/2}$ as in JM.[3] The ratio of this timescale to the rotational adjustment timescale is a nondimensional parameter, which should govern large-scale aspects of the patch:

$$\frac{f^{-1}}{t_{\text{mix}}} = H^{-1}B^{1/2}f^{-3/2} = R_o^*. \tag{5}$$

We see that this ratio is just the natural Rossby number, which was the central parameter for the *plume* scaling in JM and appears again here with a complementary interpretation of particular relevance for the *patch* scale. Its inverse measures the number of rotational adjustments that can occur during one overturning timescale [an estimate for this number is $(2\pi R_o^*)^{-1}$ since the adjustment timescale is $2\pi/f$]. The above expression for t_{mix} implies that it takes longer to carry water to the bottom the smaller is R_o^*, as is readily observed in the experiments presented in JM. This interpretation of R_o^* and the concept of the mixing timescale t_{mix} may be important to the successful parameterization of the large-scale effects of convection. An adjustment scheme, in which properties are mixed in the vertical instantaneously, is commonly adopted in numerical models and may not reproduce large-scale aspects correctly (see section 5b).

A further consequence of the rotational inhibition of vertical mixing and of the finite mixing timescale is the enhanced unstable (!) vertical density gradient maintained during cooling, particularly if R_o^* is small. This is confirmed by the numerical results described in JM. In fact, the top–bottom density difference can be scaled to be

$$g'_{\text{vertical}} \sim (Bf)^{1/2} \tag{6}$$

by a variety of physical arguments. For example, suppose that during a time t the buoyancy loss B at the surface is distributed over a depth h; then $g' \sim Bt/h$. Using the mixing timescale concept, this depth is $h = u_{\text{rot}}t$ and we obtain (6). Physically it means that for a given t considered the buoyancy extracted is proportional to t, but so is the depth over which it is distributed. Thus, a steady state is possible with the above constant vertical gradient. Perhaps not surprisingly, this g'_{vertical} has the same dependence on B and f as the density difference between plume interior and exterior (as scaled in JM).

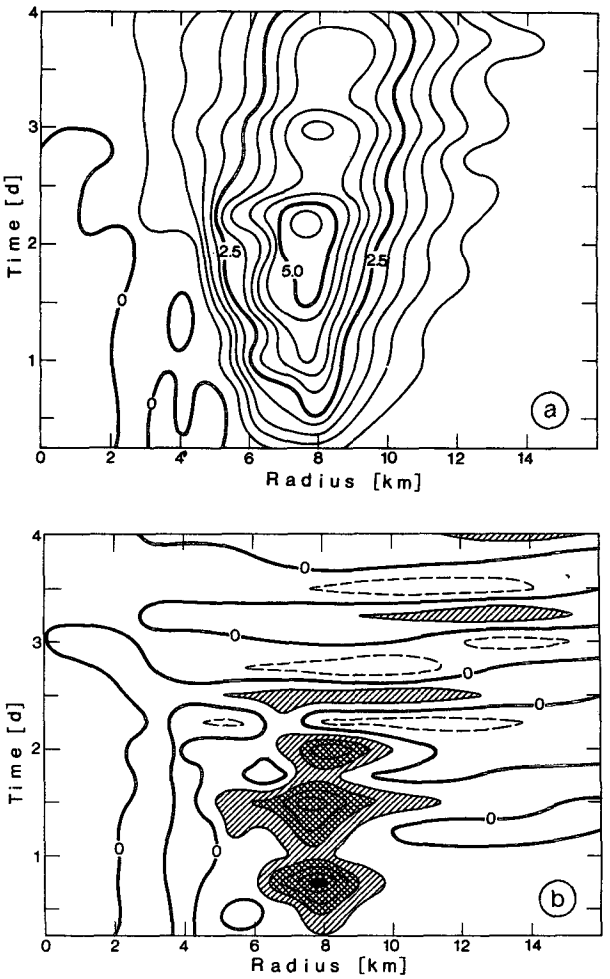

FIG. 5. Contour maps of relative vorticity and vertical velocity for the calculations shown in Figs. 3 and 4, *integrated* over disks of radius 0–16 km from 0–4 days in time. (a) Integrated relative vorticity, in units of 1000 $m^2\ s^{-1}$. At a radius of 8 km, the contour label ×2 gives (approximately) the average current around the circle, i.e., the rim current in cm s^{-1}. Note that within 5–6 km, the average vorticity averages to zero. (b) Integrated vertical velocity (i.e., vertical transport over the disk). The contour interval is 12.5×10^4 $m^3\ s^{-1}$, and this corresponds (approximately) to a disk-averaged vertical velocity of 0.5 mm s^{-1} at radius 8 km. Values larger than one such unit are shaded. Again, the velocity averages to zero within 4–6 km radius.

b. *Rim current*

The rim current generated around the edge of the convection regime is a measure of its large-scale properties. For example, the rim current must be in thermal wind balance with the density gradient between patch interior and exterior. Furthermore, its circulation is a measure of the integrated effect of all vertical velocities in the interior

[3] We are assuming here that the natural Rossby number of the convective layer R_o^* is small enough that rotational scalings are appropriate. This is certainly true in the numerical experiments in JM, who observe a transition to rotational control at $R_o^* = 0.7 - 0.8$. However, in the laboratory, the transition is observed at a somewhat smaller value of $R_o^* \approx 0.1$ (e.g., Maxworthy and Narimousa 1994). This discrepancy may be a consequence of the differences in the (eddy) diffusive processes at work in the numerical model and laboratory fluid (see Klinger and Marshall 1994). If nonrotating scaling is adopted, $w_{\text{plume}} = (BH)^{1/3}$, the expression in (5) becomes $f^{-1}/t_{\text{mix}} = R_o^{*2/3}$. Since in deep convection R_o^* lies somewhere between 0.1 and 1 and, furthermore, when $R_o^* = 1$ rotating, and nonrotating scales are equivalent, our results are only slightly modified if nonrotating scaling is adopted. We use rotating scaling here because it is the most appropriate for interpretation of our numerical experiment.

of the patch. At the same time, the existence of the rim current is of vital importance for the breakup of the patch, and its details (amplitude, width, vertical structure) might be relevant for the water exchange process by instability eddies and cones. We now use the above ideas, and in particular the concept of a mixing timescale t_{mix}, to derive key properties of the rim current.

We exploit our interpretation of $(2\pi R_o^*)^{-1}$ as a measure of the number of continuously occurring adjustments that take place during the cooling, before overturning can balance horizontal displacements associated with the sinking and slumping of the chimney under the influence of rotation and gravity. This represents the continuous inward ageostrophic motion [noted already by Killworth (1976)], which results from the ongoing cooling of the interior. The implied width of the rim current is then $(2\pi R_o^*)^{-1}$ times the Rossby radius, that would result from a single adjustment, based on the $g' = Bt/H$ at the time considered:

$$L_{rim} \sim \frac{R_o^{*-1}}{2\pi}\frac{\sqrt{g'H}}{f} = \frac{R_o^{*-1}}{2\pi}\frac{\sqrt{Bt}}{f} = \frac{H}{2\pi}(ft)^{1/2}. \quad (7)$$

Now employing thermal wind to estimate the rim current velocity, we find that

$$u_{rim} \sim \frac{1}{2}\frac{g'H}{fL_{rim}} = \pi BH^{-1}f^{-3/2}t^{1/2} = \pi R_o^* B^{1/2}t^{1/2}, \quad (8)$$

where the shear is assumed to exist between surface and middepth (where the rim current goes to zero or reverses).

The time dependence of the rim current given by (8) is in broad agreement with the JM simulations, as can be seen from Fig. 5a where the integrated vorticity was contoured over disks of increasing radius from the center of the chimney. This is also a measure of the circulation integral around circles of varying radii; the value at its maximum ($\sim$8 km) gives an estimate of the average rim current around the convection patch at that radius. Table 2, calculated from the data contoured in Fig. 5a, shows that this line integral does evolve in timelike $\sqrt{t}$ in the model and thus is in agreement with (8). According to (1), the average vertical velocity is the time derivative of the rim current velocity and should thus go like $(\sqrt{t})^{-1}$. This decrease of w with time is also observed in Fig. 5. The unknown constant of proportionality in (8) may now be estimated with the help of Table 2 and is found to be approximately 1/2. Because of (7) and (8), this also implies a constant of 2 in L_{rim} and t_{mix}. Therefore, the expressions for u_{rim}, L_{rim}, and t_{mix} become

$$u_{rim} = \frac{\pi}{2}R_o^* B^{1/2}t^{1/2}, \quad l_{rim} = \frac{H}{\pi}(ft)^{1/2},$$
$$t_{mix} = 2(fR_o^*)^{-1}. \quad (9)$$

Such a time dependence of u_{rim} and $\bar{w}$ would be difficult to explain, for example, as the sum of all the individual downwelling plume circulations since in the JM model the number of plumes remains approximately constant in time and their scaling u_{rot}, l_{rot}, l_ρ is also constant. It should also be said that the heton model of Legg and Marshall (1993), which considered the convection to be represented by a collection of discrete, paired vortices, is not able to reproduce a rim current with such a time dependence. In their point vortex model, the current is built up as the integrated effect of point vortices of like sign in each layer and its strength increases linearly with time.

TABLE 2. Rim current time dependence.

	t(d)				
	0	0.5	1.0	1.5	2.0
u_{rim}(cm s^{-1})	0	5.0	8.0	9.9	10.9
$u_{rim}/\sqrt{t}$	0	7.1	8.0	8.1	7.7

c. The Chimney breakup timescale

The rim current scaling (8)/(9) suggests that the current grows like $\sqrt{t}$ until either the applied cooling ceases or the convection patch breaks up baroclinically and disperses. Let us consider what happens if the cooling persists and baroclinic instability halts the increase in the rim current. [Such baroclinic instability of a convection chimney is a process observed in nature (e.g., see Gascard 1978).]

Invoking baroclinic instability theory, the growth rate of the most unstable mode is (Eady 1949)[4]

$$\omega_{Eady} = \frac{0.3f}{\sqrt{\mathrm{Ri}}}, \quad (10)$$

where $\mathrm{Ri} = N^2/(du_{rim}/dz)^2$ is the Richardson number associated with the persistent large-scale flow set up by the convection (i.e., the rim current). Here we interpret N^2 and du_{rim}/dz as the (constant) Brunt–Väissälä frequency and velocity shears, respectively, associated with the rim current. The timescale implied by the above is, therefore,

$$t_{Eady} = \frac{\pi}{0.3}\frac{\sqrt{g'H}}{fu_{rim}} = 3.3\pi\frac{\sqrt{Bt}}{fu_{rim}} \sim 6.6HB^{-1/2}f^{1/2}$$
$$= 6.6(fR_o^*)^{-1}, \quad (11)$$

where we have substituted for u_{rim} from Eq. (9). Hence, t_{Eady} has the same dependence on B, f, and H as t_{mix}, to which it is proportional.

Since the patch apparently breaks up via the instability of the rim current, the breakup timescale should

[4] It is not obvious a priori that this result can be applied to the present problem. However, we assume it can and investigate the consequences.

scale like this t_{Eady}. To determine the appropriate constant of proportionality, the reference experiment of JM was repeated, but now cooling persisted for 6 days. Both rim current and interior density were found to grow with the expected rate (like $\sqrt{t}$ for the current and like t for the density) until about day 4, after which a distinct slowdown was observed and at which point the cones have left the cooling region. This is demonstrated in Fig. 6, showing the 200-m flow field and the 1000-m temperature anomaly after 4 days and 6 days of cooling. At 4 days, the cones are just beginning to leave the cooling region; at 6 days they are well outside, exchanging a substantial amount of fluid with the patch. The coldest water (occupying at least 10% of the cooling area) at 1000 m has an anomaly of 0.03°–0.035°C at 4 days, while at 6 days it has only slightly increased to 0.035°–0.04°C. The absolute maxima are 0.04°–0.045°C in both cases. Constant depth-distributed cooling over the patch would predict 0.034°C at 4 days and 0.051°C at 6 days. Thus, between 4 and 6 days the mean temperature of the patch levels off by exchanging water with the surroundings—this is the time we will use as our estimate of the breakup timescale t_{breakup}. Applying (11) to the simulation shown in Fig. 6, t_{Eady} is approximately 2.5 days. This suggests to fix the constant of proportionality in (11) to yield

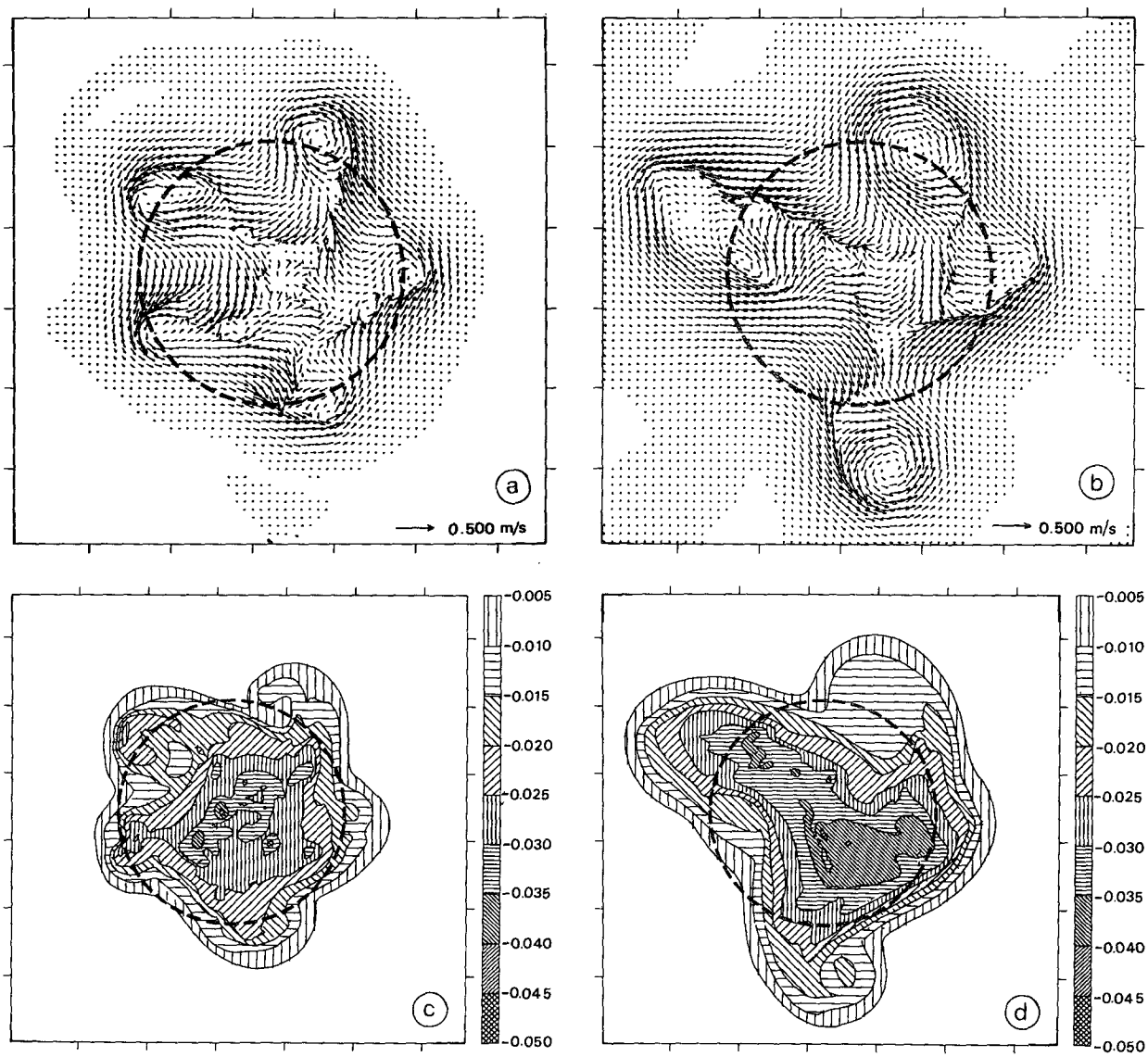

FIG. 6. Horizontal maps from the unstratified reference experiment of JM ($B = 3.6 \times 10^{-7}$ m^2 s^{-3}, $f = 10^{-4}$ s^{-1}, $H = 2000$ m), in which the cooling period was extended to 6 days of continuous cooling. The size of the cooling region is indicated and shows the cones removing cooled fluid from the patch. (a) Flow field at 200 m, day 4; (b) flow field at 200 m, day 6; (c) temperature anomaly (°C) at 1000 m, day 4; and (d) same as (c) but at day 6.

$$t_{\text{breakup}} \approx 2t_{\text{Eady}}. \quad (12)$$

Thus, at the breakup of the patch its buoyancy deficit becomes

$$g'_{\text{final}} = \frac{B}{H} t_{\text{breakup}} = 13.2(Bf)^{1/2} \quad (13)$$

and the rim current

$$u_{\text{rim,final}} = \frac{\pi}{2}\frac{B}{H} f^{-3/2} t_{\text{breakup}}^{1/2}$$

$$= 5.7B^{3/4}H^{-1/2}f^{-5/4} = 5.7fHR_o^{*3/2}. \quad (14)$$

Note that the g'_{final} is just proportional to the g'_{rot} from JM; that is, the density contrast of the patch with its exterior has the same dependencies as that of the plumes in the patch interior but is an order of magnitude larger.

The length scale of the instability scales with the deformation radius L_ρ, the wavelength of the most unstable mode being $4L_\rho$ (Pedlosky 1982). We take one-half of this wavelength for the size L_{Eady} of an eddy developing from this instability. Using the g' at t_{Eady} for estimating L_ρ then gives

$$L_{\text{Eady}} = 2\frac{\sqrt{6.6(Bf)^{1/2}H}}{f}$$

$$= 5.1H^{1/2}B^{1/4}f^{-3/4} = 5.1H\sqrt{R_o^*}. \quad (15)$$

Pleasingly, all the above proportionalities at breakup turn out to be the same as those used or obtained in JM, where, unlike here, steady-state assumptions were made. Also, in the present derivation, the physical and dynamical processes that lead to the scalings are perhaps more clearly revealed and the proportionality factors (which may not be of order unity) now result mainly from the physical derivation. In JM, for example, it was implicitly assumed that the g'_{rot} from the plumes applies to the patch as well. Here we derive that (at breakup) they are indeed proportional but with a factor of 13. Our velocity scale u_{rim} corresponds to JM's u_{cone}, for which the proportionalities again are the same. Jones and Marshall do not give a constant of proportionality, but their figure with experimental results suggests a constant of at least 3. We obtain 5.7 from our derivation, the difference arising probably from JM's method of measuring u_{cone} (rms value over some region of the model domain). Finally, in JM, $l_{\text{cone}} = 5H\sqrt{R_o^*}$, the constant resulting from a fit to the experiment. This length scale corresponds to and agrees with our above L_{Eady}. Unlike JM, we differentiate between the initial instabilities (L_{Eady}) and the later developing cones (see below), which have detached from the patch.

The width of the rim current at breakup becomes

$$L_{\text{rim,final}} = \frac{H}{\pi}(ft_{\text{breakup}})^{1/2}$$

$$= \frac{\sqrt{13.2}}{\pi} B^{-1/4}H^{3/2}f^{3/4} \approx H/\sqrt{R_o^*}. \quad (16)$$

Here L_{rim} is connected with g', u_{rim} by thermal wind balance, which is not the case for L_{Eady}.

d. Scales of the rim current, cones, and eddies

The new length scale introduced above, L_{rim}, has a positive f dependence suggesting that the baroclinic zone that circles the convection patch would widen if the rotation rate of the earth were increased. This is a curious result, especially since now we have two length scales (L_{Eady}, L_{rim}) with opposite f (and B) dependences. Scales such as the Rossby deformation radius, the instability length scale, or diffusive boundary layers *decrease* with increasing rotation, but apparently the width of the baroclinic zone *increases*. Figure 7 documents this prediction with a simulation at five times the reference rotation rate. There we observe a short-scale instability on a very wide rim current zone, as would be anticipated from the relations obtained for L_{Eady} and L_{rim}.

Of these two length scales we would expect the rim current width to be the more relevant one for the ultimate size of the developing cones, since L_{rim} describes the width of the baroclinic zone. In particular, if the rim-current strength is an appropriate measure of the swirl velocity associated with the cones, then thermal wind balance requires a cone scale of L_{rim} rather than

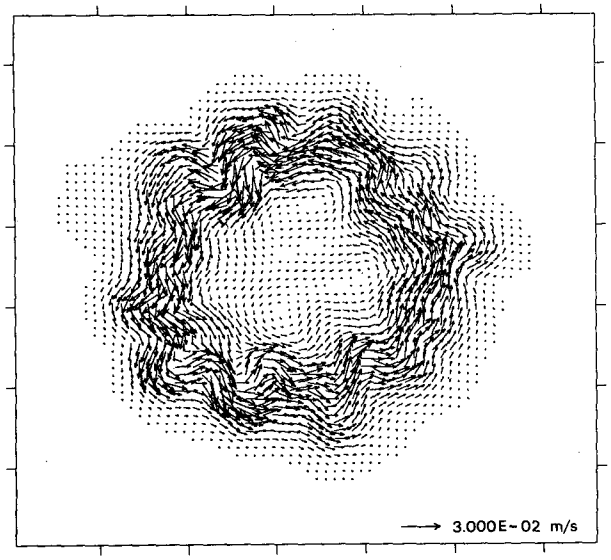

FIG. 7. Horizontal flow field at 200 m, on day 4 of a simulation in which standard cooling was applied but at high rotation: $f = 5 \times 10^{-4}$ s^{-1}. Note the large width and small strength of the rim current and the short length scale instability developing on it.

L_{Eady}. Therefore, we suggest L_{rim} as the appropriate cone radius scale, or $2L_{rim}$ for their overall size. Such a cone scale, however, would imply that if the initial instabilities form eddies of size L_{Eady} (often smaller than $2L_{rim}$), then they must later merge to form cones of size $2L_{rim}$. This should occur at small B or high f. Section 4 will present such a merger process observed in a simulation at low B and will demonstrate the effect of B on the length scales.

e. *Typical numbers*

Let us insert some values into the derived relations for some of the simulations used here and in JM to obtain a feeling for the resulting scales. Table 3 gives an overview.

The first column in Table 3 is the reference run from JM. The mixing timescale for that case is $t_{mix} = 18.5^h$, and the time dependence of rim-current strength and width is $u_{rim} = 8.3 \times \sqrt{\text{days}}$ cm s^{-1}, $L_{rim} = 1.9 \times \sqrt{\text{days}}$ km. The instability eddy length scale becomes $L_{Eady} = 5.5$ km, and the breakup timescale $t_{breakup} = 5$ d. Since the cooling was switched off after 2 days, that is, well before the breakup time, the time-dependent scaling at $t = 2$ days should be used and yields 12 cm s^{-1} for the rim current. This, of course, agrees with the values calculated from Fig. 5 (Table 2), since that run was used to determine the constant of proportionality. Also the constant for $t_{breakup}$ was determined by extending that simulation and therefore cannot serve as a test for the scalings. The wavelength for the instability is a good test, however, and it reproduces the wavenumber 5 resulting in the reference case (Fig. 6). Also, the final temperature anomaly is well reproduced (Fig. 6).

Further, we discussed a high-rotation run from JM (Fig. 7), to which column 4 of Table 3 refers. There, the rim current is observed to have an amplitude of only 2 cm s^{-1}, a large width (>5 km), and a short instability of wavenumber 12. All properties are approximately predicted by the scaling if one uses the

TABLE 3. Large-scale patch properties suggested by our scaling for $H = 2000$ m.

		$Q(W\,m^{-2})$				
		800	1600	200	800	800
		$B_o(m^2\,s^{-3})$				
		3.6×10^{-7}	7.2×10^{-7}	0.9×10^{-7}	3.6×10^{-7}	3.6×10^{-7}
		$f(s^{-1})$				
		1.0×10^{-4}	1.0×10^{-4}	1.0×10^{-4}	5.0×10^{-4}	0.5×10^{-4}
		R_o^*				
Scaling		0.3	0.42	0.15	0.027	0.85
t_{mix}(h)	$2(fR_o^*)^{-1}$	18.5	13.1	37	41.4	13.1
$u_{rim}(t)$(cm s^{-1})	$\frac{\pi}{2} R_o^*(Bt)^{1/2}$	$8.3\sqrt{\text{days}}$	$16.6\sqrt{\text{days}}$	$2.1\sqrt{\text{days}}$	$0.75\sqrt{\text{days}}$	$23.5\sqrt{\text{days}}$
$u_{rim,final}$(cm s^{-1})	$5.7fHR_o^{*3/2}$	18.7	31.4	6.6	2.5	44.5
$L_{rim}(t)$(km)	$\frac{H}{\pi}(ft)^{1/2}$	$1.9\sqrt{\text{days}}$	$1.9\sqrt{\text{days}}$	$1.9\sqrt{\text{days}}$	$4.2\sqrt{\text{days}}$	$1.3\sqrt{\text{days}}$
$L_{rim,final}$(km)	$H/\sqrt{R_o^*}$	4.3	3.5	5.9	14	2.5
L_{Eady}(km)	$5.1H\sqrt{R_o^*}$	5.5	6.5	3.8	1.6	9.2
wavenumber[a]	$\frac{50.2\text{ km}}{2L_{Eady}}$	4–5	4	6–7	15	3
$t_{breakup}$(days)	$13.2(fR_o^*)^{-1}$	5	3.5	10	11.2	3.5
$\Delta T(t)$(°C)[b]	$\frac{B}{\epsilon gH}t$	.008 × days	.016 × days	.002 × days	.008 × days	.008 × days
ΔT_{final}(°C)	$\frac{B}{\epsilon gH}t_{breakup}$	0.04	0.056	0.02	0.09	0.028

[a] Wavenumber of the instability for a circular patch of radius 8 km.
[b] Temperature anomaly, $\Delta T = \epsilon g'/g$, $\epsilon = 2 \times 10^{-4}$ K^{-1}, as used in the model.

time-dependent expressions with $t = 2$ days, the cooling period.

In section 4 we will present two further simulations, cooling at twice the reference cooling rate (column 2 of Table 3) for 1 day and at 1/4 of the standard cooling (column 3) for 8 days. The main differences are the breakup timescales, which are predicted at 3.5^d and 10^d, agreeing approximately with the simulations (Figs. 8 and 9) and the instability wavenumbers, predicted as 4 and 6–7. We observe wavenumbers 5 and 7–8.

Finally, a low-rotation run presented in JM is included in column 5 of Table 3. No figures are reproduced here, but in JM the rim current is found to exceed 20 cm s^{-1}, and a very low wavenumber seems to develop there (Fig. 9f of JM), in agreement with our predictions.

In general, the instability wavenumber is a robust test of the scaling results, and the wide range from wavenumber 12 to 3 in the six simulations of JM's Fig. 9 [covering $f = 0.5 \cdots (5 \times 10^{-4}\ s^{-1})$] is very well predicted by (15). Three of those are columns 1, 4, and 5 in Table 3.

4. Lateral exchange by geostrophic eddies

Two limiting cases were identified in the previous sections: one in which the cooling is applied for a time that is much shorter than the breakup timescale of the chimney, and one in which it is applied for a time that is very much longer. Here we present two numerical experiments in which an unstratified ocean of a depth of 2 km is cooled over a disc at its upper surface in the

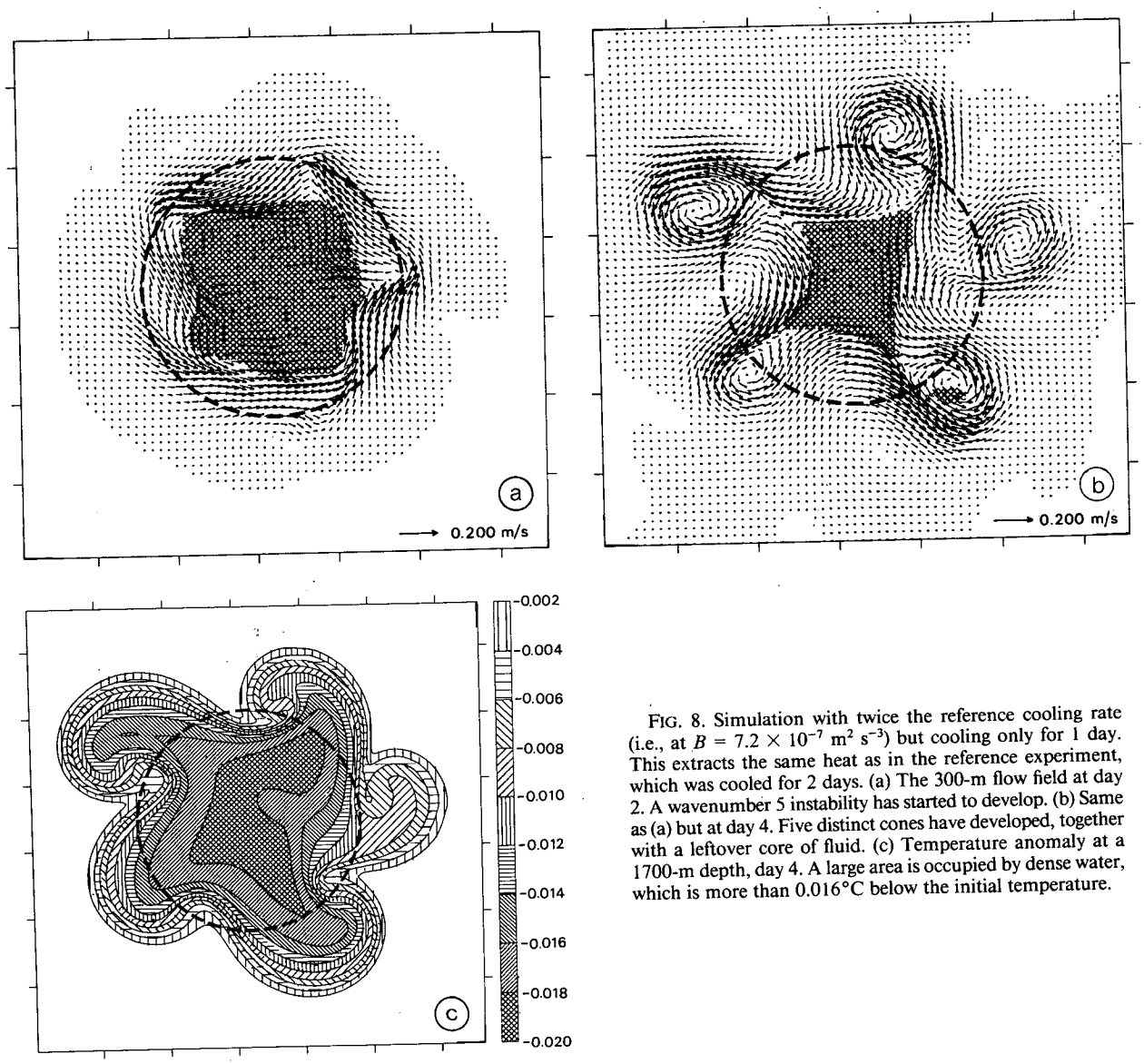

FIG. 8. Simulation with twice the reference cooling rate (i.e., at $B = 7.2 \times 10^{-7}\ m^2\ s^{-3}$) but cooling only for 1 day. This extracts the same heat as in the reference experiment, which was cooled for 2 days. (a) The 300-m flow field at day 2. A wavenumber 5 instability has started to develop. (b) Same as (a) but at day 4. Five distinct cones have developed, together with a leftover core of fluid. (c) Temperature anomaly at a 1700-m depth, day 4. A large area is occupied by dense water, which is more than 0.016°C below the initial temperature.

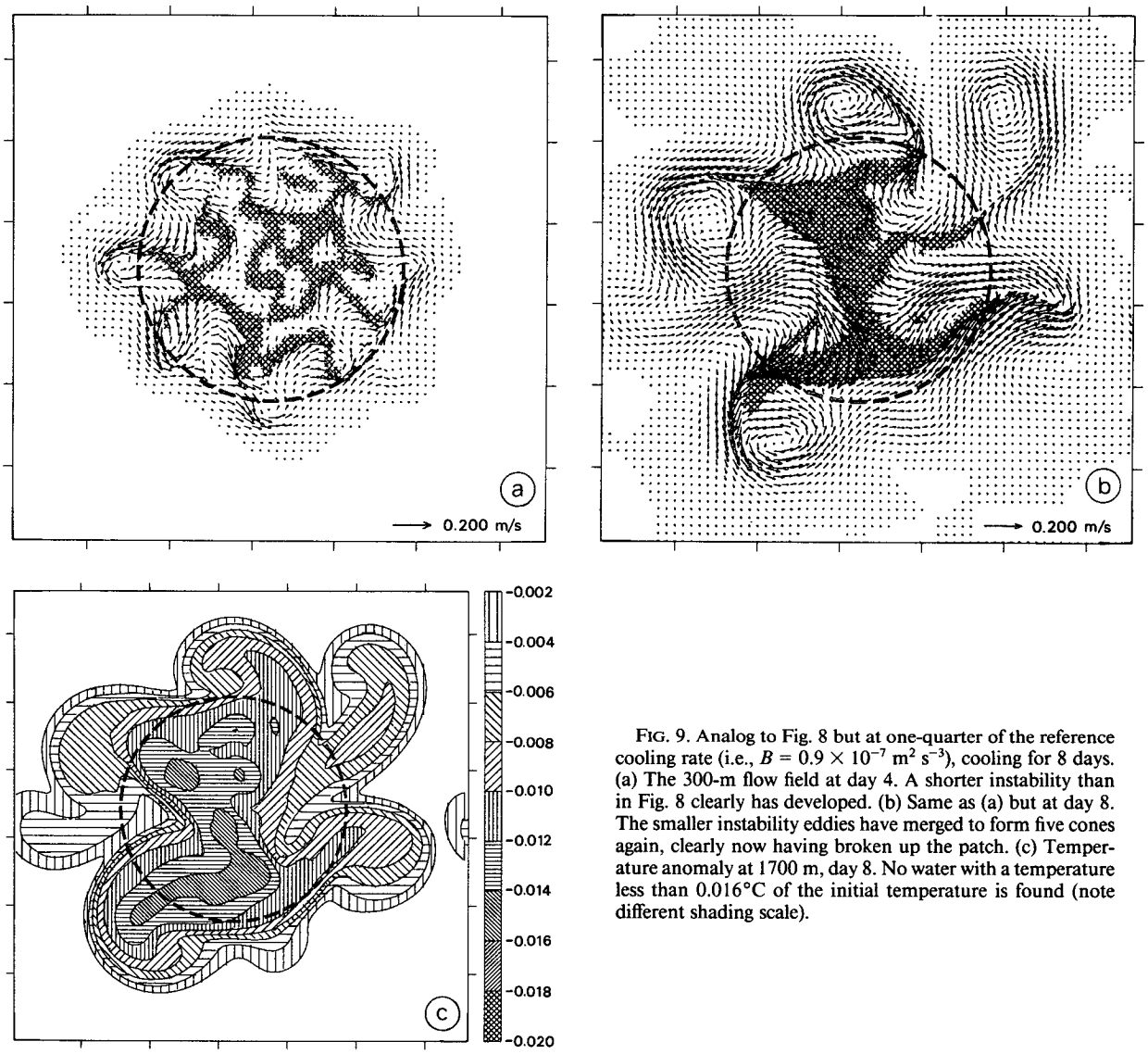

FIG. 9. Analog to Fig. 8 but at one-quarter of the reference cooling rate (i.e., $B = 0.9 \times 10^{-7}$ m^2 s^{-3}), cooling for 8 days. (a) The 300-m flow field at day 4. A shorter instability than in Fig. 8 clearly has developed. (b) Same as (a) but at day 8. The smaller instability eddies have merged to form five cones again, clearly now having broken up the patch. (c) Temperature anomaly at 1700 m, day 8. No water with a temperature less than 0.016°C of the initial temperature is found (note different shading scale).

manner described in JM and shown in their Fig. 3. In each case, 2.8×10^{16} J of heat is extracted in total. However, in the first it is extracted in 1 day (shorter than the breakup time) and in the second in 8 days (all the way through the breakup).[5]

a. Rapid cooling

In the rapidly cooled experiment (Table 3, column 2), the cooling is terminated well before breakup and even before instability development. For the given $B = 7.2 \times 10^{-7}$ m^2 s^{-1}, the breakup timescale suggested by (11) and (12) is 3.5 d. This is verified by the two horizontal maps at 2 days and at 4 days (Fig. 8a,b). In the former, the instability is just developing; by day 4 it has formed isolated eddies (cones). Thus, we should use the time-dependent scalings (9) with the cooling period inserted for t rather than the solutions (13)–(16), where t is set by the breakup timescale. The cooling period is, in fact, of the order of a rotational adjustment timescale, so we might expect this to be even a limiting case between the two-step cylinder collapse and the continuous time-dependent scaling derived above. Applying the time-dependent scaling in (9), we obtain a rim current of 14 cm s^{-1}, which is in agreement with the observed current of 12–14 cm s^{-1}. Reassuringly, the (smoothed) cylinder collapse solution ($\frac{1}{2}\sqrt{g'H}$) gives a similar value of 12.5 cm s^{-1}. The strong

[5] The reference experiment of JM was cooled for 2 days at 800 W m^2, and so, again, extracted the same total amount of heat as in the two experiments here.

cooling has generated a core of very cold water (Fig. 8c)—a volume integration gives approximately 1.2×10^{11} m^3 of water cooler than 0.016°C below the initial value.

b. Prolonged cooling

In the prolonged cooling experiment (Table 3, column 3), the time for complete breakup predicted by (12) is similar to the cooling period. This is borne out by Figs. 9a,b, showing horizontal maps at 4 days and 8 days. At 4 days, a small-scale instability has developed, but most of the cooled water is still inside the cooling disk and the patch has not yet broken up. At 8 days, we are left with five large cones now all outside the cooling area. This result not only confirms the much longer breakup timescale (observed to be 8 days, predicted by our scaling to be 10 days) but, in particular, the scale change from short instabilities (L_{Eady}) to large cones, which was predicted above by associating $2L_{\text{rim}}$ with the cone scale. The dependence of the cone size on the cooling period however is not as strong as expected since by (9) we would expect cones 2–3 times larger for the 8-day cooling case compared to the 1-day cooling. This mismatch might arise because the slow-cooling cones are exhausting the water supply, the development is not yet complete, or because the actual g' in the cones may be somewhat smaller than Bt/H. The cone/rim currents observed are 6–8 cm s^{-1}, which compares well with the scaling of (14) giving 7 cm s^{-1}. At day 8 the cones have left the influence of the cooling region and prolonged cooling will not change them any further; breakup has been reached. Since during the cooling some water has already been removed by the breakup, we would expect a greater volume of less dense water to be processed by the chimney than in the quick-cooling case. This seems to be the case (see Fig. 9c). The volume of water cooler than 0.016°C below the initial value is approximately 1.5×10^{10} m^3, only 14% of the high-cooling case.

These comparisons demonstrate the importance of the lateral exchange by the breakup eddies (cones). Depending on the strength and the length of the cooling, different amounts of water are processed and different water mass properties result. This is true in spite of removing the same total amount of heat.

5. Consequences and implications

a. Deep-water formation rate

We have argued that the large-scale effect of deep convection plume activity is best viewed simply as an overturning process that results in water mass transformations by mixing surface water (made denser by a surface buoyancy flux) with the water masses below. Time or spatially averaged vertical velocities are only associated with the slumping during rotational adjustment, are concentrated near the perimeter, and cause negligible vertical transports. Over a period of typically one to a few weeks, a fragmented convection patch results with a number of cones containing convected water from top to bottom, spinning in geostrophic balance. This dense water is likely to eventually slump to the depth at which its density matches that of the surroundings through continued instability, spindown of the eddies, or bleeding by a boundary current. Instability certainly is one process that lowers the potential energy and center of mass of the dense water formed. The detailed physics and dynamics that control the slumping and spreading phase, however, is an outstanding question, which remains to be articulated. A model example of the first stage of this process can be seen in Figs. 10a and 10b, which show the same cone at 4 days and at 6 days in an experiment with continuous cooling (after having left the cooling region); heavy water is slumping toward the bottom, and lighter water is moving in sideways at the top.

The foregoing mechanism for supplying water to the deep layer suggests that the extra amount of deep water supplied in the convection process can be computed from the volume of mixed and processed water inside the patch and cones *above* the climatological level of the deep water. This volume later settles down into the deep-water pool. Depending on the duration of the cooling and the efficiency with which fluid is exchanged by the chimney with its surroundings, this may be larger than the volume of the convective chimney, as discussed in section 4.

A related issue is that the actual deep-water replenishment need not be confined to the convection region itself. The breakup eddies (cones) can propagate away from the patch and carry dense water in various directions before final sinking or bleeding takes place. This stage has not been observed in the short simulations presented here and in JM but is suggested in related studies (Legg and Marshall 1993; Helfrich and Send 1988).

b. Convection plume parameterization

We have suggested that the large-scale effect of plumes can be regarded as an efficient vertical overturning and mixing process. If the patch dynamics and water mass formation rates are insensitive to the details of the small-scale plumes, it may be possible to parameterize their gross effect by use of a suitable mixing or convective adjustment scheme and retain realistic macroscale vertical velocities, instabilities, and water mass distributions. In particular, hydrostatic models (with an appropriate vertical exchange mechanism) may be able to produce the large-scale effects—vertical velocities by "geostrophic" slumping, rim currents by continuing rotational adjustment, and cones by baroclinic instability. If these assumptions are correct, then, for example, the large-scale relative vorticity field generated should be similar in hydrostatic and nonhydrostatic

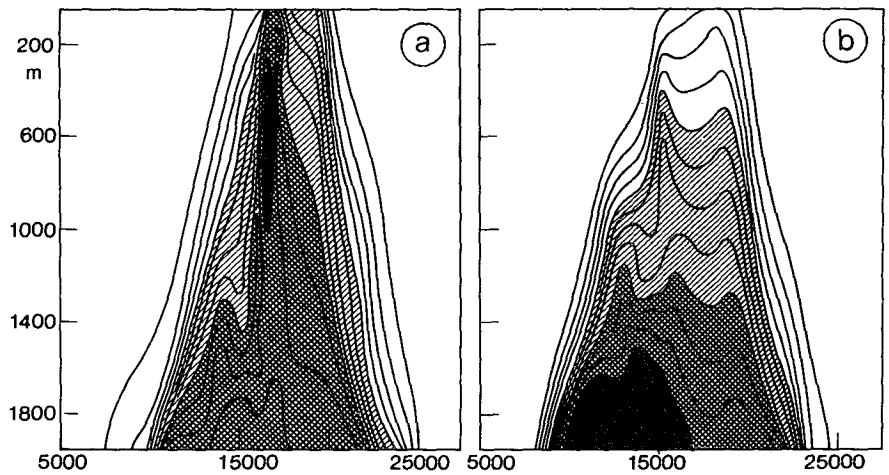

FIG. 10. Temperature cross sections across a cone for the experiment of Fig. 6, at 4 days and 6 days (the topmost cone of Figs. 6a,b, respectively). Contour interval is 0.02°C. Temperature anomalies of 0.01°, 0.018°, and 0.024°C are shaded with increasing intensities. The settling of the heavy water to the bottom (after the cone is no longer subject to the cooling) is clearly seen, together with restratification in the top layers.

models, in particular with respect to the absence of mean vorticity in the patch interior. As a test, in Fig. 11 we present the relative vorticity field from the Madec et al. (1991) hydrostatic model of MEDOC convection (see legend for more details). It should be compared with analogous diagnostics of JM's nonhydrostatic simulation shown in Fig. 5a where the convection is resolved. The parameters (size, cooling, intermittency, geometry, stratification, and convective adjustment scheme) make a quantitative comparison inappropriate, but the salient large-scale features are so similar qualitatively that it supports the idea that it may not be necessary to resolve the details of the plume dynamics.

In our scaling results for the dynamics of the rim current (width, instability length, and timescales, etc.), the essential ingredient was the interplay of t_{mix} and the rotational timescale. This suggests that it is important to reproduce the mixing timescale t_{mix} in a plume parameterization scheme to model those large-scale convection effects quantitatively. For a diffusive-type parameterization, where the relation between mixing depth and time is $h \sim \sqrt{\pi K_v t}$, this can be achieved by inserting t_{mix} from (9) and H to obtain an "effective" diffusivity of

$$K_v \sim (2\pi)^{-1} H B^{1/2} f^{-1/2}. \qquad (17)$$

This diffusivity should be "switched on" in a model when convection forced by surface fluxes results in a statically unstable water column. Some tuning of the constant of proportionality would be necessary by comparison of hydrostatic and nonhydrostatic models. A diffusive-type parameterization may not, however, be as appropriate as an adjustment/entrainment scheme that advances vertically with the above time-scale because in the latter the vertical advance is linear in time (as with plumes advancing vertically at a speed u_{rot}), while the use of a diffusivity implies a $t^{1/2}$ time dependence.

c. *Detecting convection in vorticity measurements*

Since (localized) sinking of water should generate relative vorticity, there has been hope that vorticity measurements can be used to observe and possibly quantify convection processes in the ocean. This may be true on the plume scale, where we observe (at least in the models) vorticity signatures exceeding the planetary vorticity. If there is also mean vorticity generation

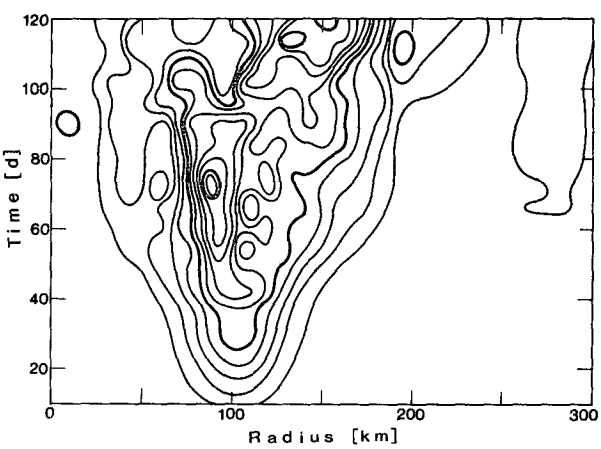

FIG. 11. Relative vorticity at a depth of 10 m integrated over ovals (their cooling shape) of radius of 0–300 km, for days 0–120, of the MEDOC simulation by Madec et al. (1991). Contour interval is 2000 $m^2 s^{-1}$.

on the large scale, this may be detectable, for example, with an acoustic tomography array arranged around or within the convection region, as employed in an experiment carried out in winter 1992/93 in the MEDOC region (The THETIS Group 1994).

We have shown above that one must expect vorticity to be concentrated in the rather narrow, sinuous band of the rim current that is meandering in space and time. If that were the case, it would be difficult to detect a circulation signal with a tomography array since the sound would have to travel much of its path within this band. If the sound path was too much within or outside the convection patch, one would not expect a robust vorticity signal based on the ideas presented here. No vorticity estimates from the above experiment are available to date, but they are awaited with interest.

It should be noted, however, that relative vorticity must be generated on a longer timescale as a consequence of the slow slumping of heavy water to the bottom and of the spreading of vorticity by the instability eddies and cones. However, in the small periodic model domain used here and in JM the horizontally averaged vorticity must remain zero at each level.

6. Discussion and summary

We have demonstrated using both physical arguments and model simulations that the convective activity in the interior of an open-ocean cooling region does not generate significant systematic vertical motion. Vorticity constraints on the large scale imply that the mean $\bar{w}$ would have to be much less than 0.01 cm s^{-1}, insignificant for deep-water formation rates and not even measurable with modern instrumentation. Even if $\bar{w}$ reached this upper limit, sheared flows of 0.5 m s^{-1} would result over a patch of 100-km size and would have a large signature in the density field associated with it. These conclusions are independent of the detailed plume properties and dynamics.

We suggest that for cooling events that are not too long compared to breakup timescales, the additional volume of new deep water formed is given merely by that of the mixed chimney above the climatological level of the deep water. This idea is, in fact, not new: Sankey (1973) estimated the amount of deep-water formation by this method. Using numbers for typical Mediterranean conditions—an area of 100 km squared and taking the upper 1000 m for the depth occupied by additional dense water—we arrive at a volume of 10^{13} m^3 per event. With only one event per year, we obtain an average of 0.3 Sv over the year, which is the currently accepted value for the Mediterranean deep-water formation rate. The length (if shorter than $t_{breakup}$) and strength of the event will not affect the amount of deep water formed; rather it will modify the temperature of the deep water generated somewhat. Its main properties are set, however, by the mixture of water types and the amount and nature of the cooling during preconditioning. We may, thus, expect year-to-year variations in the properties of the deep water formed.

If the gross dynamical and water mass modification effect of the plumes is indeed merely achieved by vertical mixing, it should be possible to parameterize the process in numerical models. Qualitative comparison of the plume-resolving JM model with the hydrostatic model by Madec et al. (1991) supported this proposition. For quantitative agreement, we have argued that it may be important to use a mixing parameterization or vertical adjustment scheme, which contains the timescale t_{mix}, or preferably a vertical "mixing speed" that corresponds to the advance rate of the plume $w_{plume} \sim u_{rot}$. Furthermore, we have suggested how one may modify existing mixing schemes by making the diffusivity depend in a particular way on B, H, and f. Such a diffusivity would be "turned on" in a model when the columns become statically unstable and R_o^* is small. For the reference case in JM ($f = 10^{-4}$ s^{-1}, $B = 3.6 \times 10^{-7}$, i.e., 800 W m^{-2}, $H = 2000$ m) we obtain a $t_{mix} \sim 18.5^h$ and, thus, a $K_v \sim 20$ m^2 s^{-1}. Some finer tuning would certainly have to be required, guided by numerical experiments, to achieve optimal agreement with plume-resolving models. We wish to emphasize that this (or an appropriately modified adjustment scheme) is only the very simplest parameterization that would be broadly consistent with our observations and scalings.

Breakup of the convection patch by instability of the rim current forms isolated cones that can carry the dense water formed away from the convection region. This was found to be an important (horizontal) exchange process. In the case of continued cooling, it could balance the cooling applied in the convection region and lead to a steady state in which the density of the water in the chimney no longer continued to increase (see also Legg and Marshall 1993). Thus, greater volumes of water are processed by the chimney through the action of the cones. Since these geostrophic eddy processes are difficult to parameterize, models containing convection processes should attempt to resolve them. The newly formed water in those spinning cones is likely to eventually slump to its neutrally buoyant level. The first stage of this slumping is probably the recapping by stratified water moving in sideways, as observed by Schott and Leaman (1991). These isolated blobs of new water should, thus, be indentifiable for some length of time after the convection, but eventually, perhaps over a number of years, they must become mixed into the deep pool of water.

Based only on the external parameters B, f, and H, we have derived scaling laws for all the large-scale properties of the convection region using physical balances instead of merely dimensional analysis. Key properties of the chimney are the rim current width and strength, the instability length and timescale, and the cone scale. There is generally good support for these

relations from the numerical model described in JM. Observational support is harder to obtain, but typical rim currents appear to be of 10 cm s^{-1} (Schott et al. 1994), as expected from the scaling. An important element in the derivations was the use of the overturning timescale t_{mix}, which measures the number of rotational adjustments possible during that time. The success of the scaling suggests the relevance of this timescale. An interesting result was the emergence of two separate spatial scales, which suggested the possibility of eddy merger to form larger cones. This was observed in the model and, apparently, also in laboratory experiments, as noted by Maxworthy and Narimousa (1994).

The sketch in Fig. 12 summarizes the various stages and length scales that have emerged from our analysis. Initially, $t < 2\pi f$, plumes comprising the convection chimney vertically mix the water column with compensating upward motion between them (solid arrows). Within an inertial period ($t \geq 2\pi/f$) continuous geostrophic adjustment resulting from the increasing density of the interior generates a vertical circulation cell concentrated near the edge of the chimney (open arrows). This results in a narrow geostrophic rim current whose vorticity is in balance with generation through stretching from the "slumping" motion associated with the geostrophic adjustment. The mixing timescale t_{mix} for vertical overturning by the plumes limits the effect of the repeated adjustment and, thus, limits the width of the rim current and the associated density gradient. After an Eady timescale, $t_{Eady} = 6.6H(f/B)^{1/2}$, meanders of length scale $L_{Eady} = 5H\sqrt{R_o^*}$ develop. These eddies may form cones of size $2L_{rim} = 2H/\sqrt{R_o^*}$, (through a merging process) and break up the patch at $t_{breakup} \approx 2t_{Eady}$. The heavy water in these cones,

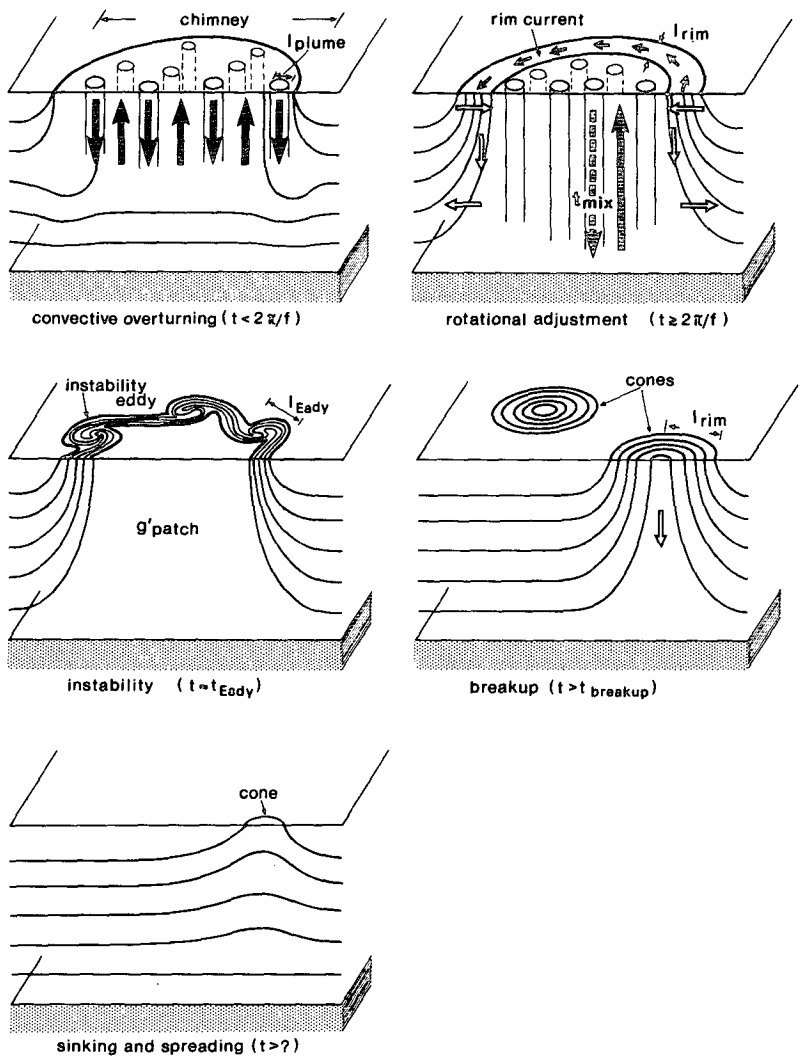

FIG. 12. Summary sketch of the various stages and properties of the convection process discussed in the text.

which may propagate away from the formation site, eventually slumps down to its neutrally buoyant level, thus adding extra volume to the deep-water pool.

All the scaling laws and most model runs assumed unstratified conditions. For weakly stratified conditions, only one example was shown, which gave very similar results in terms of vertical velocity, vorticity, and rim-current strength. This suggests that the derived relations still apply for weakly stratified cases ($N < f$). Further study is under way to understand the integral effects of convection in a stratified ocean when N is much greater than f. The most important qualitative effect of stratification may be to confine the actual convection region by setting a preconditioning scale. The size of the convection region and, thus, the deep-water formation rate will be set less by the spatial scale of the atmospheric cooling than by the area where the stratification allows a break through of the convection.

Acknowledgments. G. Madec and M. Crepon from LODYC/Paris generously provided very helpful data from their numerical model for various analyses. One such result is presented here in Fig. 11 for comparison. This study owes a great deal to T. Yates, who was supported by the MAST Mermaids project, and C. Mertens who skillfully aided in the programming, and to A. Eisele for expert drafting work. Plots were generated with FERRET, a package produced at NOAA. U. Send's work was supported by the European Community Marine Science and Technology Program, Contract MAST-0008C. John Marshall received support from the NOAA Climate Change Programme and the Office of Naval Research.

REFERENCES

Brickman, D., and D. E. Kelley, 1993: Development of convection in a rotating fluid: Scales and patterns of motion. *Dyn. Atmos. Oceans,* **19,** 389–405.

Bryden, H. L., and H. M. Stommel, 1982: Origin of the Mediterranean Outflow. *J. Mar. Res.,* **40**(Suppl.), 55–71.

Dewar, W., and P. Killworth, 1990: On the cylindrical collapse problem, mixing and the merger of isolated eddies. *J. Phys. Oceanogr.,* **20,** 1563–1575.

Eady, E. T., 1949: Long waves and cyclone waves. *Tellus,* **1,** 33–52.

Gascard, J.-C., 1973: Vertical motions in a region of deep water formation. *Deep-Sea Res.,* **20,** 1011–1027.

——, 1978: Mediterranean deep water formation, baroclinic instability, and oceanic eddies. *Oceanol. Acta,* **1,** 315–330.

Helfrich, K. R., and U. Send, 1988: Finite-amplitude evolution of two-layer geostrophic vortices. *J. Fluid Mech.,* **197,** 331–348.

Herman, A., and B. Owens, 1993: Energetics of gravitational adjustment for mesoscale chimneys. *J. Phys. Oceanogr.,* **23,** 346–371.

Jones, H., and J. Marshall, 1993: Convection with rotation in a neutral ocean: A study of open-ocean deep convection. *J. Phys. Oceanogr.,* **23,** 1009–1039.

Killworth, P. D., 1976: The mixing and spreading phases of MEDOC: 1. *Progress in Oceanography,* Vol. 7, Pergamon, 59–90.

Klinger, B. A., and J. Marshall, 1994: Regimes and scaling laws for rotating deep convection in the ocean. *Dyn. Atmos. Oceans,* in press.

Leaman, K. D., and F. A. Schott, 1991: Hydrographic structure of the convection regime in the Gulf of Lion: Winter 1987. *J. Phys. Oceanogr.,* **21,** 575–598.

Legg, S., and J. Marshall, 1993: A heton model of the spreading phase of open-ocean deep convection. *J. Phys. Oceanogr.,* **23**(6), 1040–1056.

Madec, G., M. Chartier, and M. Crepon, 1991: The effect of thermohaline forcing variability on deep water formation in the western Mediterranean Sea: A high-resolution three-dimensional numerical study. *Dyn. Atmos. Oceans,* **15,** 301–332.

Marshall, J., J. A. Whitehead, and T. Yates, 1994: Laboratory and numerical experiments in oceanic convection. *Ocean Processes on Climate Dynamics,* P. Malanotte-Rizzoli and A. Robinson, Eds., Kluwer, 173–201.

Maxworthy, T., and S. Narimousa, 1994: Unsteady, turbulent convection into a homogeneous, rotating fluid, with oceanographic application. *J. Phys. Oceanogr.,* **24,** 865–887.

MEDOC Group, 1970: Observation of formation of deep water in the Mediterranean. *Nature,* **227,** 1037–1040.

Pedlosky, J., 1982: *Geophysical Fluid Dynamics.* Springer-Verlag, 624 pp.

Sankey, T., 1973: The formation of deep water in the northwestern Mediterranean. *Progress in Oceanography,* Vol. 6, Pergamon, 159–179.

Schott, F., and K. D. Leaman, 1991: Observations with Moored Acoustic Doppler Current Profilers in the Convection Regime in the Golfe du Lion. *J. Phys. Oceanogr.,* **21,** 558–574.

——, M. Visbeck, and J. Fischer, 1993: Observations of vertical currents and convection in the central Greenland Sea during the winter of 1988/89. *J. Geophys. Res.,* **98**(C8), 14 401–14 421.

——, ——, and U. Send, 1994: Open-ocean deep convection, Mediterranean and Greenland Seas. *Ocean Processes on Climate Dynamics,* P. Malanotte-Rizzoli and A. Robinson, Eds., Kluwer, 203–225.

THETIS Group, 1994: Open-ocean deep convection explored in the Mediterranean. *Eos,* **75**(19), 217–221.

Voorhis, A. D., and D. C. Webb, 1970: Large vertical currents observed in a winter sinking region of the northwestern Mediterranean. *Cah. Oceanogr.,* **22,** 571–580.